Towards Direct Electroanalysis in Seawater: Understanding the Role of the Buffer Capacity of Seawater in Proton-Coupled Electron Transfer Reactions

Rachel L. Pindar, Christopher Batchelor-McAuley, Minjun Yang and Richard G. Compton [*]

Authors:
Rachel L. Pindar -
Physical and Theoretical Chemistry Laboratory
Department of Chemistry,
University of Oxford, OX1 3QZ

Christopher Batchelor-McAuley -
Physical and Theoretical Chemistry Laboratory
Department of Chemistry,
University of Oxford, OX1 3QZ

MinjunYang -
Physical and Theoretical Chemistry Laboratory
Department of Chemistry,
University of Oxford, OX1 3QZ

Corresponding Author:
Richard G. Compton -
Physical and Theoretical Chemistry Laboratory
Department of Chemistry,
University of Oxford, OX1 3QZ
richard.compton@chem.ox.ac.uk

Abstract

The study of electrochemical reactions in seawater requires understanding of the associated coupled chemistry with the components of seawater, especially the role of the carbonate-bicarbonate buffer system in the case of proton coupled electron transfer reactions. We report the comparative paradigmatic voltammetric response of the reversible hydrogen oxidation reaction (HOR) in the absence or presence of dibasic phosphate, formate or bicarbonate. Electrochemically and chemically reversible voltammetry is seen in aqueous 0.7 M NaCl at platinum macro-electrodes in the absence of a buffer whilst the presence of a chemically stable buffer systems, such as phosphate or formate, leads either to a cathodic shift in the oxidation potential for high buffer concentrations or to a split wave for concentrations approximately a factor of two less than the dissolved H_2. In the case of bicarbonate buffer the dehydration of carbonic acid on the voltammetric timescale leads to chemically irreversible voltammetric behaviour, with a similar response measured in authentic seawater. Numerical simulations based on a simple Nernstian model with literature values for kinetic and thermodynamic parameters are reported which display excellent agreement with experiment.

Keywords: Seawater, carbonate-bicarbonate buffer, hydrogen oxidation reaction, voltammetry, finite difference simulation

---

1. Introduction

Acidification, warming, deoxygenation, pollution, eutrophication and habitat destruction are just some of the changes being driven by human activity in the oceanic ecosystem.[1] Given that the world's oceans produce 50% of the global oxygen[2] and sequester carbon dioxide at a rate comparable to that released anthropogenically[3], understanding and monitoring these physical and biochemical changes is of global importance. However, the oceanic biochemical systems are complex and gaining a greater understanding of these systems will likely require the further development and deployment of autonomous and mobile instrumentation capable of gathering data on a global scale.[1] To address these challenges new low-power and robust sensor systems suitable for long term use under harsh and corrosive conditions are required. At present many of the used sensors systems are light based relying on optical[4], spectrometric[5] or fluorometric[6] measurements. Some measurements do utilise other technologies, a prime example being the measurement of the seawater pH using ion-sensitive field-effect transistors[7] or the detection of fish and mammals using echo location[8].

Given that seawater is highly ionically conductive with an ionic strength of ~0.7 M, direct amperometric measurements made in seawater samples seem like a good candidate technology for use as a low-cost and low energy method for chemically monitoring the marine environment. Amperometry operates through application of a potential to a working electrode which, for a suitably designed system, results in an analytically useful current being passed allowing the concentration of an analyte to be determined. Portable electrochemical systems for the voltammetric detection of heavy metals are commercially available[9] and allow field measurements of labile trace metal detection in the parts per billion range or lower[10]. However, for many electrochemical systems the analytical signal of interest is often coupled with proton transfer[11] so that the analytical signal is sensitive to the pH of the analysis solution. The use of redox indicators that are pH sensitive gives a direct route by which amperometric methods can be used to measure the pH of a sample.[12] However, if an electrochemical system is only weakly buffered then during the course of an electrochemical reaction the pH at the electrode surface can differ from that of the bulk solution. This change in pH can cause changes in the voltammetric response.[13] Primarily due to these issues for over a

hundred years the modus operandi of the electroanalytical research community has been to almost entirely focus on studying redox processes in solutions with a high enough buffering capacity to ensure that the interfacial pH remains essentially constant during an electrochemical reaction.[14] By doing so the complexity of the problem is simplified leading to results that are more readily analysable. In the absence or presence of only limited buffer concentrations the amperometric results can often be more difficult to interpret. As will be explored below this raises a problem for the use of analytical techniques directly in seawater; seawater has a pH of ~8.2 but has only a relatively low buffering capacity (reported to be in the sub millimolar range[15]), low enough to interfere with electroanalytical reactions.

The pH of seawater is predominantly controlled by the bicarbonate buffer system. Other important species such as borate are present at significantly lower concentrations.[16, 17] The total dissolved inorganic carbon content ($[CO_2(aq)] + [H_2CO_3] + [HCO_3^-] + [CO_3^{2-}]$) varies generally for seawater from 1.8 to 2.3 mmol kg^{-1} but can be up to 4.3 mmol kg^{-1} in the Dead Sea.[15] The main pH controlling equilibria are:

$$H_2O(l) + CO_2(aq) \rightleftarrows H_2CO_3(aq) \qquad K_{eq} = 1.18\text{x}10^{-3} \qquad \text{(Eq. 1)}$$

$$H_2CO_3(aq) \rightleftharpoons HCO_3^-(aq) + H^+(aq) \qquad K_{a1} = 1.18\text{x}10^{-3}\ M \qquad \text{(Eq. 2)}$$

$$HCO_3^-(aq) \rightleftharpoons CO_3^{2-}(aq) + H^+(aq) \qquad K_{a2} = 1.1\text{x}10^{-9}\ M \qquad \text{(Eq. 3)}$$

The above equilibrium constants are given as their values at a salinity close to that of seawater[17, 18] (see SI section 1) and for equation 1 the concentration of water is taken as a constant such that the equilibrium constant is the ratio of the concentrations of carbonic acid to carbon dioxide. Importantly the equilibrium for the hydration of dissolved CO_2 (Eq. 1) lies heavily to the left in favour of carbon dioxide; consequently, once formed carbonic acid rapidly falls apart to form dissolved CO_2 (rate constant, k = 10-30 s^{-1})[16, 18] and, as will be important later, implies the 'reverse' hydration of CO_2 is relatively sluggish. It should be noted that the 'true' pK_{a1} (Eq. 2) of carbonic acid is, in saline solution, ~3. However, due to the fact that carbonic acid is in equilibrium with carbon dioxide, bicarbonate behaves as a stronger base than it would if it was not chemically unstable, where:

$$H_2O(l) + CO_2(aq) \rightleftharpoons HCO_3^-(aq) + H^+(aq) \qquad K_a^* = 1.4x10^{-6}\ M \qquad \text{(Eq. 4)}$$

This reaction has an effective pKa* of 5.9 in saline solution, the term "effective" is used to signify that Eq. 4 is the composite of two reactions, the protonation of bicarbonate and the dehydration of carbonic acid.[17] Furthermore, although bicarbonate can act as a stronger base its behaviour is in part dependent upon the timescale under investigation. At short-times relative to the equilibration of equation 1, bicarbonate acts as a base where the conjugate acid has a pK_a of 2.9 but at longer times it behaves as a base with a conjugate acid of pK_a of 5.9. This switch in behaviour depends on the kinetics of equation 1 relative to the timescale of the experiment. At short times bicarbonate can be protonated but there is insufficient time for the dehydration step to occur. Conversely, at longer times the dehydration of carbonic acid serves to pull reaction 2 over increasing the "apparent "or "effective" strength of the base.

The fact that the concentration of the buffer in seawater is limited to millimolar concentrations and that the kinetics of the hydration of CO_2 are relatively sluggish (as compared to the voltammetric timescale of seconds) means that seawater is a complicated buffering system for amperometric measurements. Recently, the importance of the bicarbonate acid-base equilibria for electrochemical CO_2 reduction has become recognised.[19] However, in this work we focus not on the direct electrochemistry of dissolved inorganic carbon but seek to investigate how the buffering influences and changes the voltammetric response of proton coupled electron transfer (PCET) reactions. In this paper we first present theory which outlines how the addition of a base to the solution is anticipated to influence the voltammetric response of an electrochemical PCET reaction, taking the hydrogen (H_2) oxidation reaction as a paradigmatic example of such a PCET process. Second, we experimentally study the HOR under differing buffering conditions. As will be demonstrated, the hydrogen oxidation is an *electrochemically reversible* system at a platinum macroelectrode in the presence of simple bases such as phosphate and formate. In contrast, under buffering conditions which mimic that of seawater the reaction becomes *chemically irreversible* on the voltammetric timescale.

2. Experimental Methods

2.1 Chemicals.

Hydrogen (≥99.98%) was supplied from BOC, Surrey, UK. All other chemicals supplied from Sigma-Aldrich, Dorset. All solutions were made with ultrapure water from Millipore with resistivity not less than 18.2 MΩ cm at 298 K.

2.2 Electrochemistry.

A three electrode system in a Faraday cage was used for all electrochemical experiments. A lab built low noise potentiostat was used as previously described. A low noise variable gain amplifier (DLPCA-200, FEMTO Messtechnik GmbH Germany) was used to convert the current to an analog voltage signal. This voltage signal was digitized at 100 KS/s via a USB data acquisition device (USB-6003, National Instruments, Austin, TX) and then filtered digitally by a four-pole Bessel filter to 250 Hz by using a script written in Python. All electrochemical measurements were thermostated at 25 ± 0.5 °C.

3. Theory

This section theoretically investigates how the voltammetric response of the hydrogen oxidation reaction (E) at a macroelectrode is influenced by the following chemical reactions (C) in each of two cases: First, the presence of a generic base X which can reversibly react with the electrochemically generated acid to form the associated conjugate acid Y (an EC reaction). Second, the presence of a generic base X that can react reversibly with the formed acid but where the formed conjugate acid Y is able to undergo a further unimolecular reaction to form species Z (an ECC reaction). In this section we assume that the kinetic and thermodynamic parameters associated with the hydrogen oxidation reaction are adequately described by the values at infinite dilution.

The hydrogen oxidation reaction is:

$$H_2 \rightleftharpoons 2H^+ + 2e^- \qquad \text{(Eq. 5)}$$

and due to the stoichiometry of the reaction the Nernst equation is[20]:

$$E = E_f + \frac{RT}{2F} \ln \frac{[H^+]^2}{[H_2][\theta]} \quad \text{(Eq. 6)}$$

where E is the electrode potential (V), E_f is the formal potential for the redox couple (V), R is the Gas Constant (8.314 J K^{-1} mol^{-1}), T is the temperature (298 K), F is the Faraday constant (96485 C mol^{-1}) and [θ] is the standard concentration (1 mol dm^{-3}). Importantly, the formal potential is defined at unit concentration whereas the standard potential is defined at standard conditions. At standard pressure (1.013 bar) the saturated concentration of hydrogen in water is 0.784 mM (the Henry's law constant 1292 dm^3 mol^{-1} bar^{-1}[21]). Due to this relatively low solubility of hydrogen in water these two definitions of the potential (standard vs formal) differing significantly where in the present case the formal potential (E_f) for the hydrogen/proton redox couple is -0.0918 V vs SHE (see SI section 2 for further details). Furthermore, at infinite dilution the diffusion coefficients for hydrogen and protons have been reported to be 5.1×10^{-9} m^2 s^{-1} and 9.3×10^{-9} m^2 s^{-1} respectively.[22] Under conditions where diffusion coefficients of the species are not equal then the voltammetric mid-point potential is shifted and must be accounted for in the simulation.

In the following two subsections we focus on solving the associated mass-transport problems for the i) EC and ii) ECC reactions. These reaction mechanisms have been investigated theoretically previously;[11] however, the near entirety of the literature to-date focuses on systems in which the electrochemical reaction is of unity-stoichiometry i.e. one molecule of an electroactive reagent is oxidized or reduced to form one molecule of a product. As highlighted in equation 5 the oxidation of hydrogen leads to the formation of two protons. This non-unity stoichiometry causes some subtle changes in the associated voltammetric response. First the position of the voltammetric wave is sensitive to the concentration of the redox active species and can, under some circumstances, lead to the position of a wave shifting in a manner different from that expected for a reaction with a simple 1:1 stoichiometry.[20] Second, the voltammetric wave shape differs from that of a simple reaction with 1:1 stoichiometry leading to different peak heights associated with the electrochemical process.[23]

In the following theoretical results, we assume that the surface concentrations of hydrogen and protons are fully described by the Nernst equation (Eq. 6). Further the mass-transport of species in the solution phase is assumed one-dimensional. The

coupled mass-transport, heterogeneous and homogeneous reaction problem is solved for using a central backward implicit finite difference method where the non-linear terms are solved using the Newton-Raphson method.[24] More details on the simulation procedure is presented in the SI section 3.

3.1 EC reaction

In this section we consider the case in which the formed protons can react with a base (X) present in the solution phase, the overall reaction scheme is:

$$H_2 \rightleftharpoons 2H^+ + 2e^- \qquad \text{(Eq. 7)}$$

$$H^+ + X \rightleftharpoons Y \qquad \text{(Eq. 8)}$$

The pK_a of the conjugate acid (Y) is related to the equilibrium constant for reaction 8 via the following:

$$K_{eq1} = 10^{pK_a} = \frac{[Y]}{[H^+][X]} \qquad \text{(Eq. 9)}$$

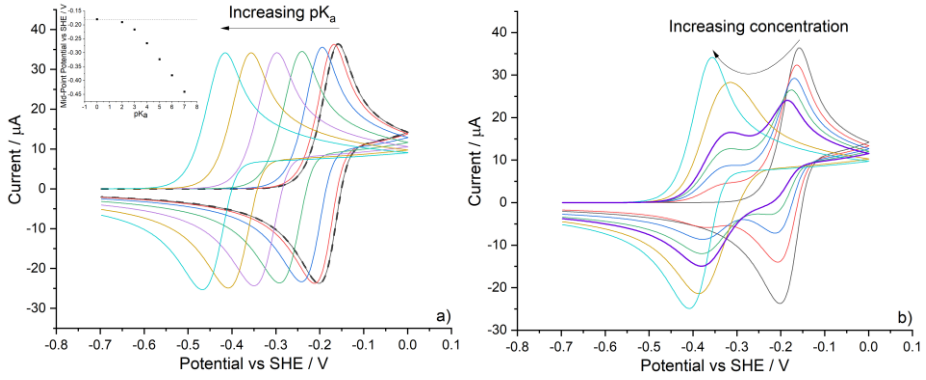

Figure 1: Simulated voltammetric response for the reversible oxidation of hydrogen and the influence of the presence of a base in the solution phase. a) Influence of the variation of the pK_a (0-7) of the base (10 mM), dotted line is predicted voltammetric response in the absence of a base: black 0; red 2, blue 3; green 4, purple 5; yellow 6; cyan 7. b) Change in the HOR voltammogram in the presence of a base with a pK_a of 6 where the base concentration has been varied from 0-10 mM: black 0 mM; red 0.5 mM; blue 1.0 mM; green 1.5 mM; purple (bold) 2.0 mM; yellow 4 mM and cyan 10 mM. $D_{H2} = 5.1 \times 10^{-9}$ m^2 s^{-1}, $D_{H+} = 9.3 \times 10^{-9}$ m^2 s^{-1}, $D_{base} = D_{acid} = 1 \times 10^{-9}$ m^2 s^{-1}, $[H_2]_{bulk} = 0.784$ mM, $E_f = -0.0918$ V (vs SHE), electrode radius = 1 mm and scan rate = 0.1 V s^{-1}.

For clarity the "pK_a of the conjugate acid" is sometimes referred to in the literature as the pK_aH. In this work when discussing the associated pK_as we refer to the pK_a of the conjugate acid. In the simulation the kinetics of protonation and deprotonation are set sufficiently fast to ensure that the processes is fully at equilibrium. The voltammetric response for the oxidation of a solution saturated with hydrogen in the presence of 10 mM base was simulated as a function of the associated pK_a of the conjugate acid. Here we assume that the diffusion coefficient for the base and conjugate acid is equal with a value of $1x10^{-9}$ m^2 s^{-1}. Figure 1 a) presents the resulting voltammograms. Also overlaid is the expected voltammetric response in the absence of a base in the solution phase (dotted line), which is essentially identical to the situation in which the conjugate acid has a pK_a of zero. The simulated voltammograms starts at -0.7 V (vs SHE) and scanned anodically to 0.0 V (vs SHE), on the forward scan a peak arises due to the oxidation of hydrogen to protons due to the process being fully reversible (by definition) a peak associated with the reduction process is observed on the reverse scan. In the absence of a base the mid-point potential for the simulated voltammogram is -0.181 V (vs SHE) as demarked by the dotted line on the inset. It is notable that this mid-point potential is significantly negative of the formal potential (-0.0918 V vs SHE). This shift arises from the fact that the formal potential is defined at unit concentration (1 M) whereas the simulation is for a saturated solution containing 0.784 mM hydrogen. Using the Nernst equation (Eq. 6) we can derive an approximate expression[20] for the expected mid-point potential of the reversible hydrogen oxidation voltammogram in the absence of base. At the mid-point potential ~50% of the hydrogen will have been consumed and will have formed a stoichiometric quantity of protons hence:

$$E_{mid} \approx E_f^{\ominus} + \frac{RT}{2F} \ln \frac{2[H_2]_{bulk}}{[\theta]} \qquad \text{(Eq. 10)}$$

This expression predicts a mid-point potential for the redox wave of -0.175 V, this is within 7 mV of the simulated mid-point potential. The deviation arises since the different known diffusion coefficients for hydrogen and protons were used in the simulation whereas the derivation of equation 10 assumes equality of the diffusion coefficients.

As can be seen from Figure 1 a) in the presence of a base the hydrogen oxidation wave is shifted negatively. The magnitude of this shift depends upon the strength of the base, or conversely the weakness of the associated acid. Note an increase in the conjugate acid pK_a is equivalent to an increase in the strength of the base. Figure 1 a) depicts how the reversible hydrogen oxidation wave is expected to shift as a function of the strength of the base present in the solution phase, where the pK_a of the conjugate acid has been used to quantify the base strength. Increasing the strength of the base makes the hydrogen oxidation reaction more thermodynamically favourable as the base binds to the electrochemically generated protons, shifting the voltammetric wave negatively. The inset of Figure 1 a) plots the mid-point potential for the hydrogen oxidation wave as a function of the conjugate acid pK_a. For pKa values above 3 the mid-point potential shifts with 59.1 mV per pK_a unit.

Figure 1 a) shows the oxidation of H_2 in excess base. The voltammetric response for the hydrogen oxidation reaction was simulated as a function of the concentration of the base. Figure 1 b) depicts the simulated results for a base with a pK_a of 6 where its concentration has been varied from 0-10 mM. At high and low concentrations, a single voltammetric wave is observed. The position of the wave reflects the underlying thermodynamics of the oxidation of hydrogen to either free proton or protonated base. However, at intermediate concentrations a split wave is observed. For example at 2 mM base (purple line in bold) two clear voltammetric peaks are observed at -0.35 and -0.2 V (vs SHE). The first peak corresponds to the oxidation of hydrogen leading to the formation of the conjugate acid. However, the concentration of the base is only finite; consequently, as the reaction proceeds the base becomes titrated away at the interface leading to a peak, the remaining hydrogen cannot then be oxidized until the electrode reaches a potential sufficient for the hydrogen to be oxidized directly to free protons. Hence the second observed peak corresponds to the oxidation of the remaining hydrogen in the absence of base. Note that if the diffusion coefficients of all the species in the simulation were all equal then the split wave would occur when the base was at an approximately equal concentration so that half of the formed protons are titrated away bound to the base. Thus the relative sizes of the two parts of the split wave directly reflects the stoichiometry of the reaction. However, in the present case this voltammetric feature occurs at a high concentration due to the relatively high diffusion

coefficient of hydrogen as compared to the base ($5.1x10^{-9}$ m^2 s^{-1} and $1x10^{-9}$ m^2 s^{-1} respectively) which leads to a greater availability of hydrogen to the electrode surface. From these results we can see, first, the position of the hydrogen oxidation wave varies as a function of both the pK_a of the conjugate acid and the concentration of the base. In all cases assuming the acid/base reaction is at equilibrium then both the hydrogen oxidation and proton reduction reaction can proceed leading to voltammetric peaks on both the forward and reverse scan. In the next section we consider the situation in which the conjugate acid can undergo a unimolecular reaction where the kinetics of this reaction are not necessarily assumed to be fast.

3.2 ECC reaction

In this section we consider the case where the formed conjugate acid (Y) can undergo a further unimolecular reaction to form species Z, the overall reaction scheme is:

$$H_2 \rightleftharpoons 2H^+ + 2e^- \quad \text{(Eq. 11)}$$

$$H^+ + X \rightleftharpoons Y \quad \text{(Eq. 12)}$$

$$Y \underset{\rightleftharpoons}{^{kf}} Z \quad \text{(Eq. 13)}$$

$$K_{eq2} = \frac{[Z]}{[Y]} \quad \text{(Eq. 14)}$$

In contrast to the acid/base reaction we do not assume that the unimolecular reaction (Eq. 13) is at equilibrium. The voltammetric response for the oxidation of hydrogen, H_2, in the presence of base with a pK_a of 3 was simulated. Further the equilibrium constant for the unimolecular reaction (Eq. 13) was set at $1x10^3$. In this simulation the forward rate constant (k_f) for the conversion of Y to Z was varied from $1x10^{-2}$ to $1x10^8$ s^{-1}. The simulated voltammetric results for this reaction scheme is presented in Figure 2 a). For slow rates less than $1x10^{-2}$ s^{-1} the unimolecular reaction has no influence on the voltammetric response and the hydrogen oxidation wave occurs at the potential expected for a base with a pK_a of 3. Conversely at high rates, greater than $1x10^8$ s^{-1}, the unimolecular reaction is fully at equilibrium consequently the voltammetric wave is shifted and appears at a potential equivalent to that of base with a conjugate acid with a pK_a of 6, where the shift in potential is given by:

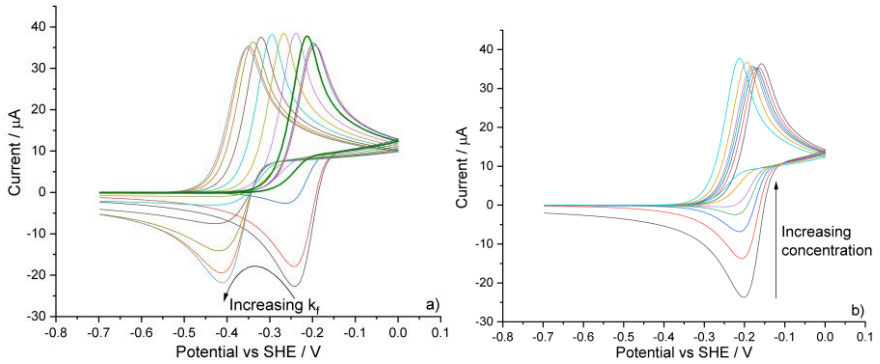

Figure 2: Simulated voltammetric response for the reversible oxidation of hydrogen and the influence of the presence of a base in the solution phase where the formed conjugate acid is able to undergo a further unimolecular reaction. a) for a fixed base concentration C_{base} = 10 mM, the influence of the forward rate constant of the unimolecular reaction where k_f is varied from $1x10^{-2}$ – $1x10^{8}$ s^{-1}: black $1x10^{-2}$ s^{-1}; red $1x10^{-1}$ s^{-1}; blue $1x10^{0}$ s^{-1}; green (bold) $1x10^{1}$ s^{-1}; purple $1x10^{2}$ s^{-1}; yellow $1x10^{3}$ s^{-1}; cyan $1x10^{4}$ s^{-1}; brown $1x10^{5}$ s^{-1}; light brown $1x10^{6}$ s^{-1}; red $1x10^{7}$ s^{-1}; blue $1x10^{8}$ s^{-1}. b) depicts the variation of the voltammetric shape as a function of the concentration of the base where the forward rate constant of the unimolecular reaction is fixed at 10 s^{-1}. Concentration of the base varied from 0-10 mM: black 0 mM; red 0.5 mM; blue 1.0 mM; green 1.5 mM; purple 2.0 mM; yellow 4.0 mM and cyan 10 mM. pK_a = 3, K_{eq2} = 1000, D_{H2} = $5.1x10^{-9}$ m^2 s^{-1}, D_{H+}= $9.3x10^{-9}$ m^2 s^{-1}, D_{base}= D_{acid}=$1x10^{-9}$ m^2 s^{-1}, $[H_2]_{bulk}$ = 0.784 mM, E_f = -0.0918 V (vs SHE), electrode radius = 1 mm and scan rate = 0.1 V s^{-1}.

$$\Delta E = \frac{2.303RT}{F} pK_a \qquad \text{(Eq. 15)}$$

Although the true pK_a of the acid used in this simulation is 3, the presence of a fast unimolecular follow up homogeneous reaction means that the pK_a of the conjugate acid is *effectively* raised. Equation 9 shows that when species Y is in equilibrium with species Z, then the equilibrium constant for the overall reaction becomes:

$$10^{pK_a + pK_{eq2}} = \frac{[Z]}{[H^+][X]} \qquad \text{(Eq. 16)}$$

where for the present example pK_{eq2} = 3, corresponding to K_{eq2} = 10^3. Hence the "effective" pK_a' = pK_a + pK_{eq2}.

The intermediate case between these two limits of a fast and slow unimolecular reaction is more complex. Although at both the very high and low kinetic limits the hydrogen oxidation process is voltammetrically reversible since a reduction peak occurs. At intermediate scan rates the oxidation is voltammetrically irreversible. An example of

this case is highlighted in Figure 2 a) for the case where $k_f = 10\ s^{-1}$ (bold green line). This irreversibility arises not from the interfacial redox kinetics being slow but occurs due to the irreversibility of the unimolecular reaction on the timescale of the voltammogram. Here the formed protons are titrated away by the base forming the conjugate acid as an intermediate, this acid subsequently reacts to form species Z. In this intermediate kinetic regime there is insufficient time during the voltammetric scan for species Z to be converted back to Y. The formed protons become kinetically trapped, under this ECC scheme the hydrogen oxidation reaction is kinetically irreversible.

Having explored how the kinetics of the unimolecular reaction rate influences the voltammetric waveshape when the base is in excess we now turn to consider the situation for the intermediate kinetic regime where the concentration of the base is finite. Figure 2 b) plots the predicted voltammetric response for the hydrogen oxidation reaction in the presence of base with a conjugate acid of pK_a of 3 and where the unimolecular reaction has an equilibrium constant of 1000 and a forward rate constant of $10\ s^{-1}$. The concentration of the base is varied from 0 – 10 mM. As can be seen from Figure 2 b) the prominent feature of these voltammograms is that as the concentration of the base is added the magnitude of the reverse peak, associated with hydrogen evolution is decreased in magnitude. Voltammetrically the base serves to titrate away the formed protons. This case, an ECC reaction, as will be exemplified later, essentially characterizes the voltammetric hydrogen oxidation reaction in the presence of bicarbonate. In the next section the work focuses on experimental verification of these theoretical results and serves to demonstrate how the presence of bicarbonate in seawater serves to render the hydrogen oxidation reaction chemically irreversible.

4. Results and Discussion

Having theoretically explored the expected behaviour for the reversible hydrogen oxidation reaction in the presence of a base this work now turns to consider experiment for comparison to theory.

First, we consider the voltammetric response of hydrogen in the absence and presence of a ‘simple’ weak base which simply accepts protons with no follow up

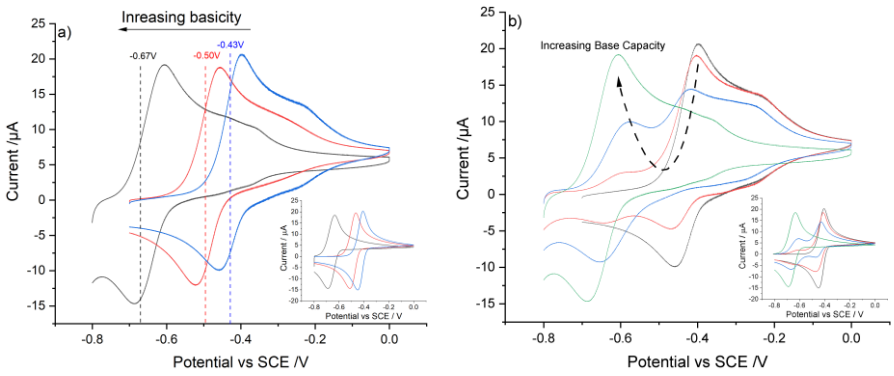

Figure 3: Voltammetric response of a platinum macroelectrode in a hydrogen saturated solution (0.7 M NaCl): a) in the absence of a base (blue) and in the presence of 10 mM formate (red line) and 10 mM dibasic phosphate. The dashed vertical lines demark the predicted mid-point potentials for the hydrogen oxidation reaction as predicted by the corresponding simulations (inset). b) in differing concentrations of dibasic phosphate 0 mM (black), 0.5 mM (red), 2 mM (blue) and 10 mM (green). Insets depict the *simulated* voltammetric results for the same set of experimental conditions. Simulation details: $[H_2]$ = 0.644 mM, $pK_{a(formate)}$ = 3.5, $pK_{a(phosphate)}$ = 6.7, D_{H2} = 4.9x10^{-9} m^2 s^{-1}, D_{H+}= 6.7x10^{-9} m^2 s^{-1}, $D_{formate}$=13.6x10^{-10} m^2 s^{-1}, $D_{phosphate}$ = 6.6x10^{-10} m^2 s^{-1}, E_f = -0.1008 V (vs SHE), electrode radius = 0.83 mm and scan rate = 0.1 V s^{-1}.

chemistry as seen for conventional buffers. Figure 3 A) depicts voltammetry of a platinum electrode in a saturated solution of hydrogen in 0.7 M NaCl, to mimic the ionic strength of seawater, in the absence of a base (blue line). Also shown is the voltammetry in the additional presence of 10 mM formate (red line) and 10 mM dibasic phosphate (black line). In all cases a reversible redox wave is observed and the presence of the base serves to make the oxidation more thermodynamically favorable shifting the redox wave negatively since the H^+ formed combines with the base. Note at higher potentials a secondary voltammetric feature is observable in the diffusional tail of the experimental voltammogram. In the absence of base (blue line) this additional feature occurs at ~-0.1V vs SCE. This feature is associated with the underpotential deposition of hydrogen onto the platinum surface[25] and is not the focus of this work. Notably the experimental use of smaller platinum surface would minimise this hydrogen underpotential deposition signal. In this work 0.7 M NaCl is used as a supporting electrolyte to provide an ionic strength comparable to that of seawater. The electrolyte serves to alter some of the thermodynamic and kinetics parameters associated with the

hydrogen oxidation process from those reported in the earlier theory section where the values used were for the species at infinite dilution and in the absence of a supporting electrolyte. More specifically the proton activity coefficient, hydrogen solubility, acid association constants and diffusion coefficients are all lowered by the presence of the electrolyte (see below). Under these ionic conditions the proton activity coefficient is approximately 0.772[26] and the solubility of the hydrogen is 0.644 mM (as calculated using a Sečenov parameter of 0.114 for NaCl[27]). This change in the thermodynamic parameters leads to a calculated formal potential for the reaction of -0.1008 V (vs SHE), a nine-millivolt shift from the formal potential reported in the theory section. Experimentally a saturated calomel electrode is used for the reference electrode[28] which differs from the SHE by -0.2411 V (E_f = -0.3419 V vs SCE). In 0.7 M NaCl the pK_as of formic acid and monobasic sodium phosphate are reported as 3.5[29] and 6.7[30] respectively (as compared to their values of 3.75 and 7.20 at infinite dilution in pure water. The diffusion coefficients of hydrogen and protons are 4.9×10^{-9} m^2 s^{-1} and 6.7×10^{-9} m^2 s^{-1} respectively.[31,32] For the other species involved in the acid/base equilibria finding exact literature values for their diffusion coefficients in seawater is more challenging. However, it has been reported for a number of ions that their diffusion coefficients are approximately 10% lower in seawater as compared to their value at infinite dilution. [33] On this basis we assume that a) all of the acid/base species have the same diffusion coefficient and that this value is 10% below that of the base at infinite dilution. Consequently, for phosphate and formate we have taken the values of 6.6×10^{-10} m^2 s^{-1} and 13.6×10^{-10} m^2 s^{-1},[34] respectively. Using these thermodynamic and kinetic parameters the voltammetric response for the reversible hydrogen oxidation reaction was simulated in the absence and presence of a base (10 mM dibasic phosphate or 10 mM formate). This is shown in the inset of Figure 2 a) and the simulated mid-point potentials for the hydrogen oxidation wave were found to be -0.429 V (vs SCE, no base). -0.496 (vs SCE, 10 mM formate) and -0.672 V (vs SCE, 10 mM dibasic phosphate). These measured mid-point potentials have been demarked on the experimental data shown in Figure 2 a). Experimentally the measured mid-point potentials are found to be -0.429 V (vs SCE, no base), -0.489 V (vs SCE, 10 mM formate) and -0.646 V (vs SCE, 10 mM dibasic phosphate). Note that although the model is relatively simple, there are no variables or unknown fitting parameters, all

variables have been set from known and reported literature values. The predicted mid-point potentials are calculated from reported thermodynamic and kinetic data. In the worst case, for dibasic phosphate, the voltammetric mid-point potential differs by less than 26 mV from that theoretically predicted. This relatively small discrepancy for the phosphate case most likely reflects the fact that the hydrogen oxidation reaction is only quasi-reversible at higher pH.[35] In the present case this decrease in the kinetics is reflected by the marginally greater experimental peak-to-peak separation for the phosphate case. The experimental HOR voltammogram in the presence of 10 mM dibasic phosphate the peak-to-peak separation is 82 mV (theoretically predicted 55 mV) as compared to 65 and 61 mV for the voltammograms in the presence of 10 mM formate and no base (theoretically expected 48 and 43 mV respectively). This increase in the peak-to-peak separation for the more basic solution containing dibasic phosphate strongly suggests that the hydrogen oxidation reaction is, under these conditions, only quasi-reversible, and hence the measured mid-point potential will not solely reflect the thermodynamics of the system. Note in all cases the experimentally larger peak-to-peak separations indicate some kinetic limitation in the reversibility of the hydrogen oxidation reaction that is not accounted for in the present model which strictly applies a Nernstian boundary condition at the interface. For the voltammograms recorded in the presence of formate and in the absence of base the difference between the experimental and theoretical mid-point potential is less than 7 mV and 1 mV respectively. This small discrepancy may reflect the fact that in the present simulation it has been assumed that the mass-transport to and from the electrode is well described as a one-dimensional system, however given the size of the electrode (radius 0.83 mm) and the high diffusion coefficients associated with both hydrogen and protons there is likely a significant edge effect.[23] This radial diffusion contribution will serve to alter the voltammetric peak shape and will alter the exact mid-point potential.

In the previous section we considered the case where the base was in excess over the concentration of hydrogen. Here we consider the case where the concentration of the base is varied. Figure 3 B) shows the voltammetric response of the hydrogen oxidation reaction as a function of the dibasic phosphate concentration ranging from 0-10 mM, also inset is the simulated response. At high (10 mM) and low (0 mM) phosphate concentrations the position of the voltammetric wave are the same as presented in

Figure 3 A). At intermediate concentrations a split voltammetric wave is observed. Taking the 0.5 mM (red) voltammogram as an example, the voltammogram starts -0.8 V vs SCE and scanned anodically. Initially at low potentials ca. -0.6 V vs SCE a peak occurs due to the oxidation of hydrogen leading to the protonation of the dibasic phosphate, once the base has been "titrated" away at the interface the rate of hydrogen oxidation becomes limited by the diffusional flux of the phosphate to the interface. As the potential increases further, the oxidation of the hydrogen to form solvated protons becomes favourable leading to a second voltammetric wave at ca. -0.4 V vs SCE. On the reverse scan two peaks are observed corresponding initially to the reduction of free protons and the then subsequently at more negative potentials the reduction of protons that were bound to the phosphate. Comparable voltammetric results have been previously reported for the reduction of quinone moieties in the presence of a finite acid concentration.[13] In conventional buffer systems, where there are no coupled homogeneous kinetics associated with the proton transfer, as evidenced here for the case of phosphate and formate, the presence of a finite buffer capacity leads to split voltammetric waves where the ratio of the peak heights reflects the relative concentrations of the analyte as compared to the buffer and the relative diffusion coefficients of the hydrogen and protons.

In summary the presented simplified theoretical model, in which we assume that the hydrogen oxidation reaction and acid/base equilibria are fully reversible and where the non-unity stoichiometry of the interfacial reaction is fully accounted for, is able to very successfully describe the voltammetric hydrogen oxidation reaction providing quantitative agreement with experiment without using any fitting parameters. Importantly the thermodynamics associated with this redox process are calculated from the definition of the standard hydrogen electrode potential. In the following we experimentally consider the case in which the base is bicarbonate, with implications for seawater.

As discussed in the introduction due to the sluggish kinetics associated with the hydration/dehydration of carbon dioxide the bicarbonate buffering system is more complex than found for many acid-base systems. The true pK_a of carbonic acid is, at an ionic strength comparable to sea water, ~3. However, due to the dehydration process (as given in equation 1) the apparent pK_a of carbon dioxide (as described by equation

4) is 5.9. We now evidence how these coupled processes effect of the system buffering on the voltammetric timescale.

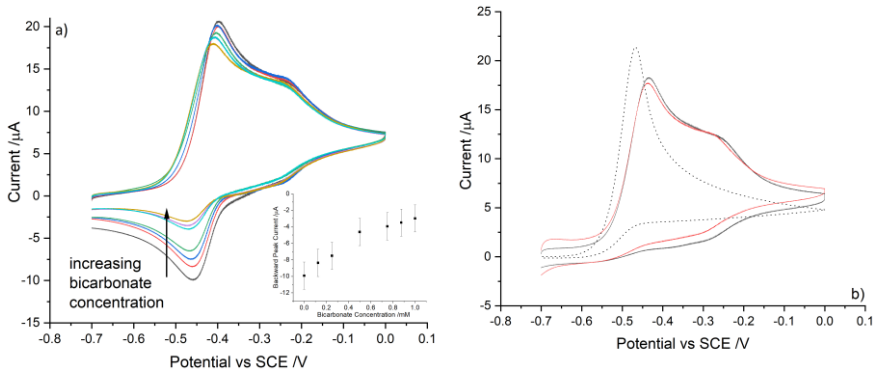

Figure 4: The oxidation of hydrogen, H_2, on a platinum macroelectrode A) voltammetry in 0.7 M NaCl in the presence of increasing concentration of bicarbonate 0-1.0 mM, inset depicts the change in the backward peak current as a function of the concentration of the base. B) Comparison of the voltammetric response in 0.7 M NaCl and 2mM bicarbonate (black), an authentic seawater sample (red) both saturated with hydrogen and the simulated voltammetric response (dehydration constant 26s^{-1}). Simulation details: [H_2] = 0.644 mM, pK_{a1} = 2.9, K_{eq2} = 868, $k_{dehydration}$ = 26 s^{-1}, D_{H2} = 4.9x10^{-9} m^2 s^{-1}, D_{H+}= 6.7x10^{-9} m^2 s^{-1}, $D_{bicarbonate}$= $D_{carbonic}$ = D_{co2} = 10.6x10^{-10} m^2 s^{-1}, E_f = -0.1008 V (vs SHE), electrode radius = 0.83 mm and scan rate = 0.1 V s^{-1}.

Figure 4 A) depicts the oxidation of hydrogen in 0.7 M NaCl with increasing bicarbonate concentrations in the range of 0 to 1.0 mM. In the absence of the bicarbonate the reversible hydrogen oxidation wave occurs at -0.43 V vs SCE. Increasing the bicarbonate concentration does not lead to the occurrence of an additional oxidative voltammetric wave at lower potentials. In the presence of a base with a pK_a of 5.9, following the results presented in the theory section, a voltammetric wave would be anticipated to occur at ~-0.64 V vs SCE. The fact that the addition of bicarbonate only causes a minor shift in the voltammetric wave immediately indicates that the base is, *on the voltammetric timescale*, significantly weaker. Note as demonstrated in the SI section 4, the minor observed shift in the voltammetric wave is fully consistent with the presence of a base with a conjugate acid of pK_a ~3. Second and most notably the addition of bicarbonate causes the magnitude of the back peak corresponding to proton reduction to decrease. Furthermore, as shown in Figure 4 B) in

the presence of 2 mM bicarbonate the back peak is essentially entirely supressed. This result in Figure 4 B) is compared with the voltammetric response of the hydrogen oxidation reaction in a genuine seawater sample (red line), again as is the case in the presence of bicarbonate there is essentially no reductive peak associated with the reduction of protons to hydrogen. This result contrasts with the data shown in Figure 3 B) where although the peaks may be thermodynamically shifted the reduction process is still feasible.

The inset of Figure 4 A) depicts the back-peak current as a function of the bicarbonate concentration. Increasing the solution phase bicarbonate concentration decreases the magnitude of the reverse peak. For the bicarbonate buffer system on the forward wave protons are formed from the oxidation of the hydrogen and the acid protonates the bicarbonate base. The formed carbonic acid rapidly dehydrates to form dissolved carbon dioxide and water (as expressed by equation 1). The first order rate constant for this dehydration step has been reported in a range of around 10-30 s^{-1} at 25°C.[18] On the back voltammetric scan the remaining free protons available in solution are reduced to hydrogen at ~-0.45 V vs SCE. However, the protons that were titrated away by the bicarbonate buffer are, on the voltammetric timescale, no longer available. The first order rate constant[16] for the hydration of CO_2 is 1.5-3x10^{-2} s^{-1} (N.B. a value of 3.07x10^{-2} s^{-1} is used in the simulation presented in Figure 4 b). Hence the effective 'release' of the proton from the electrochemically formed carbon dioxide will only occur on the time scale of tens of seconds. The experimental scan rate for the data presented in Figure 4 is 0.1 V s^{-1} hence the reductive sweep only takes a few seconds and is not long enough for the carbon dioxide/bicarbonate system to re-equilibrate. The bicarbonate essentially fully titrates away the formed protons causing the hydrogen oxidation reaction to appear irreversible.

Finally, in order to fully confirm this interpretation, the voltammetric response of a hydrogen redox couple in the presence of 2 mM sodium bicarbonate was simulated as an ECC process. Here the diffusion coefficient of bicarbonate was taken to be 5.9x10^{-10} m^2 s^{-1}, the true carbonic acid pK_a was set at 2.92 and the forward rate constant for the dehydration of carbonic acid to carbon dioxide was set at 26 s^{-1}. Although a range of values have been reported in the literature for the kinetics of the dehydration step we use the relatively more recently measured value of 26 s^{-1}. [18] The resulting

simulated voltammogram is overlaid with the data presented in Figure 4 b) (dotted line, for the simulated data as a function of bicarbonate concentration see the SI section 4). There is good agreement between the simulated and experimental voltammetry, where the primary discrepancy occurs at higher potentials (0.2-0.3 V vs SCE) and is associated with the underpotential deposition of hydrogen on the platinum surface, something that is not considered in the present theoretical model. The key point is that the simulation correctly predicts the occurrence of a *chemically irreversible* oxidation wave with a peak in current at ~-0.45 V (vs SCE). The difference in waveshape between the simulated and experimental data likely reflects the fact that in the simulation the electron transfer kinetics are assumed to be fully reversible. Note that, in the present case no consideration of the effect of possible anion-surface interactions[36] have been accounted for. In this work due to the magnitude of the currents involved the response will be dominated by bicarbonate present in the solution phase. However, if significantly lower current densities are investigated the influence of specific anion surface adsorption may become relevant. A final note of interest is that in the seawater sample additional oxidative current is observed at the foot of the main voltammetric wave. This pre-wave oxidation is associated with the presence of carbonate in the seawater sample, the higher pK_a (8.95) associated with the carbonate/bicarbonate system means that the hydrogen oxidation can occur at a lower potential. Experimentally the voltammogram cannot be started at a lower potential than approximately -0.7 V (vs SCE) due to the significant onset of solvent break down; consequently, this initial hydrogen oxidation process does not appear as a clearly defined pre-wave but simply as an apparently raised background current (see SI section 5 for further details).

5. Conclusions

The pH of a seawater sample is predominantly controlled by the bicarbonate system. From an electrochemical stand point this presents complexity due to both the relatively low (mM) concentrations of the buffering agents and the fact that once formed carbonic acid is unstable leading to the formation of carbon dioxide. In this work we presented

a simplified Nernstian model that can provide a quantitative description of the system, without additional unknowns nor requiring any 'fitting' parameters.

First, it is demonstrated how for a simple acid/buffer system the presence of a base leads to a thermodynamic shift in the hydrogen oxidation wave and that, second, when the concentration of the base is comparable to that of hydrogen a 'split-wave' is observed. The first wave in the split wave is associated with the oxidation of hydrogen to form the conjugate acid and the second wave is related to the oxidation of hydrogen to free protons- the hydrogen oxidation reaction essentially titrates away the base at the electrochemical interface.

In contrast to bases such as formate or phosphate in the presence of bicarbonate a split voltammetric wave is not observed. The protonation of bicarbonate leads on the voltammetric timescale to the irreversible oxidation of hydrogen to form dissolved carbon dioxide. These results have fundamental and applied implications for pH sensors in seawater samples that operate using amperometric detection of a redox indicator. Since such amperometric pH measurement methods necessarily alter the pH local to the electrode, without careful design the accuracy of the reported pH value may be in significant error. The above work has predominantly focused on an oxidative system in which protons are released causing the formation of dissolved carbon dioxide, for amperometric pH detection we speculate that the use of a reductive process to probe the solution phase pH has the potential to yield more accurate results.

6. Associated Content

Supporting Information:

Bicarbonate thermodynamics in high iconic strength media, the formal potential for the hydrogen/proton redox couple, Finite difference simulation details, simulated voltammetric response for the HOR in the presence of bicarbonate, experimental voltammetry of the HOR in the presence of carbonate.

7. Acknowledgement

This work was carried out with the support of the Oxford Martin School Programme on Monitoring Ocean Ecosystems. https://www.oxfordmartin.ox.ac.uk/ocean-ecosystems/

References

(1) Chai, F.; Johnson, K. S.; Claustre, H.; Xing, X.; Wang, Y.; Boss, E.; Riser, S.; Fennel, K.; Schofield, O.; Sutton, A. Monitoring ocean biogeochemistry with autonomous platforms. *Nat. Rev. Earth Environ.* **2020**, *1* (6), 315-326.
(2) Boyce, D. G.; Lewis, M. R.; Worm, B. Global phytoplankton decline over the past century. *Nature* **2010**, *466* (7306), 591-596.
(3) Milliman, J. D. Production and accumulation of calcium carbonate in the ocean: Budget of a nonsteady state. *Global Biogeochem. Cycles* **1993**, *7* (4), 927-957.
(4) Graff, J. R.; Westberry, T. K.; Milligan, A. J.; Brown, M. B.; Dall'Olmo, G.; van Dongen-Vogels, V.; Reifel, K. M.; Behrenfeld, M. J. Analytical phytoplankton carbon measurements spanning diverse ecosystems. *Deep Sea Res., Part I* **2015**, *102*, 16-25.
(5) Johnson, K. S.; Coletti, L. J.; Jannasch, H. W.; Sakamoto, C. M.; Swift, D. D.; Riser, S. C. Long-term nitrate measurements in the ocean using the In Situ Ultraviolet Spectrophotometer: sensor integration into the Apex profiling float. *J. Atmos. Oceanic Tech.* **2013**, *30* (8), 1854-1866.
(6) Roesler, C.; Uitz, J.; Claustre, H.; Boss, E.; Xing, X.; Organelli, E.; Briggs, N.; Bricaud, A.; Schmechtig, C.; Poteau, A. Recommendations for obtaining unbiased chlorophyll estimates from in situ chlorophyll fluorometers: A global analysis of WET Labs ECO sensors. *Limnol. Oceanogr.: Methods* **2017**, *15* (6), 572-585.
(7) Johnson, K. S.; Jannasch, H. W.; Coletti, L. J.; Elrod, V. A.; Martz, T. R.; Takeshita, Y.; Carlson, R. J.; Connery, J. G. Deep-Sea DuraFET: A pressure tolerant pH sensor designed for global sensor networks. *Anal. Chem.* **2016**, *88* (6), 3249-3256.
(8) Guihen, D.; Fielding, S.; Murphy, E. J.; Heywood, K. J.; Griffiths, G. An assessment of the use of ocean gliders to undertake acoustic measurements of zooplankton: the distribution and density of Antarctic krill (Euphausia superba) in the Weddell Sea. *Limnol. Oceanogr.: Methods* **2014**, *12* (6), 373-389.
(9) Trace2O. *trace2o.com*. accessed Aug 2021.
(10) Borrill, A. J.; Reily, N. E.; Macpherson, J. V. Addressing the practicalities of anodic stripping voltammetry for heavy metal detection: a tutorial review. *Analyst* **2019**, *144* (23), 6834-6849.
(11) Savéant, J. M. *Elements of Molecular and Biomolecular Electrochemistry: An Electrochemical Approach to Electron Transfer Chemistry*; Wiley, 2006.
(12) Rubinstein, I. Voltammetric pH measurements with surface-modified electrodes and a voltammetric internal reference. *Anal. Chem.* **1984**, *56* (7), 1135-1137.
(13) Batchelor-McAuley, C.; Kozub, B. R.; Menshykau, D.; Compton, R. G. Voltammetric responses of surface-bound and solution-phase anthraquinone moieties in the presence of unbuffered aqueous media. *J. Phys. Chem. C* **2011**, *115* (3), 714-718.

(14) Quan, M.; Sanchez, D.; Wasylkiw, M. F.; Smith, D. K. Voltammetry of quinones in unbuffered aqueous solution: reassessing the roles of proton transfer and hydrogen bonding in the aqueous electrochemistry of quinones. *J. Am. Chem. Soc.* **2007**, *129* (42), 12847-12856.
(15) Dickson, A. G.; Sabine, C. L.; Christian, J. R. *Guide to best practices for ocean CO2 measurements*; North Pacific Marine Science Organization, 2007.
(16) Stumm, W.; Morgan, J. J. *Aquatic Chemistry: Chemical Equilibria and Rates in Natural Waters*; Wiley, 2013.
(17) Millero, F. J. The marine inorganic carbon cycle. *Chem. Rev.* **2007**, *107* (2), 308-341.
(18) Soli, A. L.; Byrne, R. H. CO2 system hydration and dehydration kinetics and the equilibrium CO2/H2CO3 ratio in aqueous NaCl solution. *Marine chemistry* **2002**, *78* (2-3), 65-73.
(19) Marcandalli, G.; Villalba, M.; Koper, M. T. M. The Importance of Acid–Base Equilibria in Bicarbonate Electrolytes for CO2 Electrochemical Reduction and CO Reoxidation Studied on Au (hkl) Electrodes. *Langmuir* **2021**, *37* (18), 5707-5716. Costentin, C.; Robert, M.; Savéant, J.-M. Catalysis of the electrochemical reduction of carbon dioxide. *Chem. Soc. Rev.* **2013**, *42* (6), 2423-2436.
(20) Jiao, X.; Batchelor-McAuley, C.; Kätelhön, E.; Ellison, J.; Tschulik, K.; Compton, R. G. The subtleties of the reversible hydrogen evolution reaction arising from the nonunity stoichiometry. *J. Phys. Chem. C* **2015**, *119* (17), 9402-9410.
(21) Wilhelm, E.; Battino, R.; Wilcock, R. J. Low-pressure solubility of gases in liquid water. *Chem. Rev.* **1977**, *77* (2), 219-262.
(22) Lide, D. R. *CRC Handbook of Chemistry and Physics, 84th Edition*; Taylor & Francis, 2003.
(23) Kätelhön, E.; Batchelor-McAuley, C.; Compton, R. G. Voltammetric Peak Heights of the Proton–Hydrogen Redox Couple: A Comprehensive Analysis. *The Journal of Physical Chemistry C* **2015**, *119* (40), 23203-23210.
(24) Compton, R. G.; Katelhon, E.; Ward, K. R.; Laborda, E. *Understanding Voltammetry: Simulation Of Electrode Processes (Second Edition)*; World Scientific Publishing Company, 2020.
(25) Markham, J.; Young, N. P.; Batchelor-McAuley, C.; Compton, R. G. Bipolar Nanoimpact Transients: Controlling the Redox Potential of Nanoparticles in Solution. *J. Phys. Chem. C* **2020**, *124* (25), 14043-14053.
(26) Robinson, R. A.; Stokes, R. H. *Electrolyte Solutions: Second Revised Edition*; Dover Publications, 2002.
(27) Long, F. A.; McDevit, W. F. Activity coefficients of nonelectrolyte solutes in aqueous salt solutions. *Chem. Rev.* **1952**, *51* (1), 119-169.
(28) Bard, A. J.; Faulkner, L. R. *Electrochemical Methods: Fundamentals and Applications, 2nd Edition*; John Wiley & Sons, Incorporated, 2000.
(29) Harned, H. S.; Owen, B. B. The thermodynamic properties of weal acids and bases in salt solutions, and an exect method of determining thei dissociation constants. *J. Am. Chem. Soc.* **1930**, *52* (12), 5079-5091.
(30) Green, A. A. The preparation of acetate and phosphate buffer solutions of known pH and ionic strength. *J. Am. Chem. Soc.* **1933**, *55* (6), 2331-2336. Cohn, E. J. The activity coefficients of the ions in certain phosphate soutions a contribution to the theory of buffer action. *J. Am. Chem. Soc.* **1927**, *49* (1), 173-193.

(31) Jähne, B.; Heinz, G.; Dietrich, W. Measurement of the diffusion coefficients of sparingly soluble gases in water. *Journal of Geophysical Research: Oceans* **1987**, *92* (C10), 10767-10776.
(32) Roberts, N. K.; Northey, H. L. Proton and deuteron mobility in normal and heavy water solutions of electrolytes. *Journal of the Chemical Society, Faraday Transactions 1: Physical Chemistry in Condensed Phases* **1974**, *70*, 253-262.
(33) Yuan-Hui, L.; Gregory, S. Diffusion of ions in sea water and in deep-sea sediments. *Geochimica et cosmochimica acta* **1974**, *38* (5), 703-714.
(34) Bidstrup, D. E.; Geankoplis, C. J. Aqueous Molecular Diffusivities of Carboxylic Acids. *Journal of Chemical and Engineering Data* **1963**, *8* (2), 170-173.
(35) Ramaswamy, N.; Ghoshal, S.; Bates, M. K.; Jia, Q.; Li, J.; Mukerjee, S. Hydrogen oxidation reaction in alkaline media: Relationship between electrocatalysis and electrochemical double-layer structure. *Nano Energy* **2017**, *41*, 765-771.
(36) Mantelli, H.; Martinez-Hincapie, R.; Feliu, J.; Scherson, D. Potential-induced acid-base chemistry of adsorbed species. *Electrochim. Acta* **2019**, *324*, 134793.

TOC

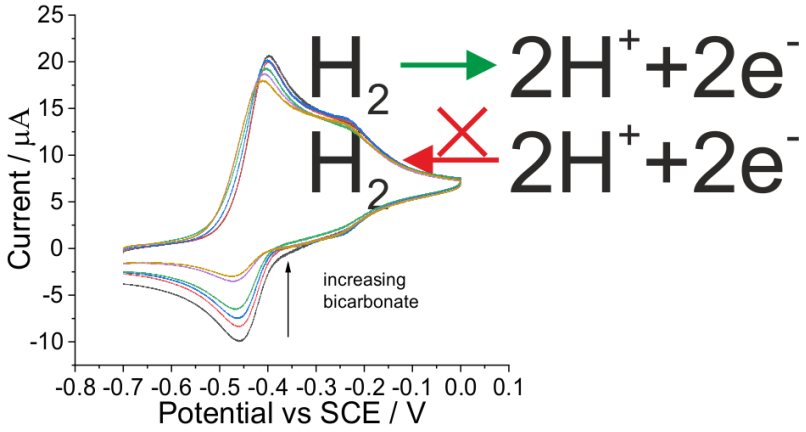
H2 → 2H+ +2e-
H2 ← 2H+ +2e-
Current / μA
Potential vs SCE / V
increasing
bicarbonate